Viscous Faraday waves in two-dimensional large-aspect-ratio containers

By FRANCISCO J. MANCEBO AND JOSÉ M. VEGA

ETSI Aeronáuticos, Universidad Politécnica de Madrid, Plaza Cardenal Cisneros 3, 28040-Madrid, Spain

A weakly nonlinear analysis of one-dimensional viscous Faraday waves in two-dimensional large-aspect-ratio containers is presented. The surface wave is coupled to a viscous long-wave mean flow that is slaved to the free-surface deformation. The relevant Ginzburg–Landau-like amplitude equations are derived from first principles, and can be of three different types, depending on the ratio between wavelength, depth and the viscous length. These three equations are new in the context of Faraday waves. The coefficients of these equations are calculated for arbitrary viscosity and compared with their counterparts in the literature for small viscosity; a discrepancy in the cubic coefficient is due to a dramatic sensitivity of this coefficient on a small wavenumber shift due to interplay between viscous effects and parametric forcing.

1. Introduction

Faraday waves (Faraday 1831; Rayleigh 1883) are parametrically excited on the fluid surface upon vertical vibration of the container when the forcing amplitude exceeds a frequency-dependent threshold value (Fauve 1995). Beyond this threshold, these waves exhibit a fairly interesting spatio-temporal behaviour (Miles & Henderson 1990; Cross & Hohenberg 1993), especially at large aspect ratio (Douady, Fauve & Thual 1989; Kudrolli & Gollub 1997; Westra, Binks & van de Water 2003). Unfortunately, several issues remain unsolved, especially (but not only) in connection with the associated mean flow, which appears when either (i) viscous effects are weak, or (ii) the aspect ratio is large. Case (i) involves a *streaming flow* produced by averaged viscous stresses in oscillatory boundary layers, which requires a fairly involved analysis, already performed in various limiting cases, at both moderate (Higuera, Vega & Knobloch 2002; Martín, Martel & Vega 2002) and large aspect ratio (Vega, Knobloch & Martel 2001; Lapuerta, Martel & Vega 2002; Vega & Knobloch 2003). This paper is concerned with case (ii) for arbitrary viscosity and can be considered as the weakly nonlinear extension of the linear analysis by Kumar & Tuckerman (1994). The mean flow in case (ii) is associated with the long wave *deformational modes* (see below) and is slaved to the free-surface deformation. This is in contrast with other mean flows that appear in, for example, strictly inviscid water waves (Davey & Stewartson 1974), Poiscuille flow (Davey, Hocking & Stewartson 1974), and Rayleigh–Benard convection (Zippelius & Siggia 1982). Most theoretical studies in the viscous limit (Beyer & Friedrich 1995; Müller *et al.* 1997; Cerda & Tirapegui 1998; Mancebo & Vega 2002) are linear. Nonlinear terms have been considered in the viscous limit only by Chen & Viñals (1999), who in fact considered
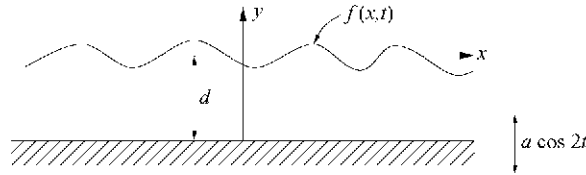
FIGURE 1. Sketch of the fluid domain.

three-dimensional deep containers, but ignored both spatial modulation and the mean flow.

The main objective of this paper is to include these two effects and calculate the relevant amplitude equations, including the quantitative calculation of the coefficients in the limits of both shallow (in §3) and deep (in §4) containers, which lead to qualitatively different equations. These equations are new and we claim that they are *the correct amplitude equations*. In addition, we shall consider the small-viscosity limit (in §3.1 and §4.1), to compare the values of the coefficients calculated in this paper with previous results in the literature, which had been controversial (Hansen & Alstrom 1997). The results compare quite well with asymptotic calculations by Mancebo & Vega (2004), who included some subtle effects at small viscosity that lead to $O(1)$-corrections in the coefficients and have not been considered before. This will completely close a long-standing controversy concerning the calculation of the cubic coefficient in deep containers; a similar analysis in shallow containers remains to be done. Section 5 gives some concluding remarks concerning the scope and consequences of the main results. For illustration, the coefficients of the amplitude equations will be calculated in some experimental conditions taken from some experiments on Faraday waves in the literature to conclude that all the limits considered in this paper are experimentally accessible.

2. Formulation

In order to clarify the role of the mean flow, we consider the restricted two-dimensional case: a laterally unbounded fluid layer with periodic boundary conditions. This is a model of a three-dimensional annular container whose width is small compared to length, but large compared to both depth and the wavelength of the excited surface waves. In this case, radial modulations and the effects of both the curvature of the annulus and the inner and outer walls (Benjamin & Scott 1979; Benjamin & Graham-Eagle 1985) are expected to be small.

We consider a horizontal fluid layer (figure 1) of unperturbed depth d^* and length L^*, which is vibrating vertically with an amplitude a^* and a frequency $2\omega^*$. We use a Cartesian coordinate system with the $y = 0$ axis at the unperturbed free surface, and non-dimensionalize length and time with $(\nu/\omega^*)^{1/2}$ and $1/\omega^*$, respectively, where ν is the kinematic viscosity. The governing equations and boundary conditions are obtained from the standard velocity–pressure formulation (Batchelor 1967) using the streamfunction ψ defined such that the velocity $(u, v) = (-\psi_y, \psi_x)$, the vorticity Ω, and the free-surface elevation f. The definition of vorticity and the momentum equations lead to

$$\psi_{xx} + \psi_{yy} = \Omega, \quad \Omega_t - \psi_y \Omega_x + \psi_x \Omega_y = \Omega_{xx} + \Omega_{yy} \quad \text{in } -d < y < f, \quad (2.1)$$

The boundary conditions at the free surface,

$$
\left.
\begin{aligned}
&\mathscr{G}f_x - \mathscr{S}\left(\frac{f_x}{\sqrt{1+f_x^2}}\right)_{xx} - \psi_{yt} + \psi_{xt}f_x - (\psi_x + \psi_y f_x)\Omega + \tfrac{1}{2}\left(\psi_x^2 + \psi_y^2\right)_x \\
&+ \tfrac{1}{2}\left(\psi_x^2 + \psi_y^2\right)_y f_x - 4af_x\cos 2t = -3\psi_{xxy} - \psi_{yyy} + (\psi_{xxx} + \psi_{xyy})f_x \\
&+ 2\left[\frac{2\psi_{xy}f_x^2 + (\psi_{xx} - \psi_{yy})f_x}{1+f_x^2}\right]_x + 2\frac{(\psi_{xxy} - \psi_{yyy})f_x^2 - \psi_{xyy}\left(1 - f_x^2\right)f_x}{1+f_x^2}, \\
&f_t - \psi_x - \psi_y f_x = 0, \quad (\psi_{yy} - \psi_{xx})\left(1 - f_x^2\right) - 4f_x\psi_{xy} = 0 \quad \text{at } y = f,
\end{aligned}
\right\}
\tag{2.2}
$$

account for the equilibrium of normal stresses, kinematic compatibility and free tangential stress, respectively. No slip at the bottom, horizontal periodicity and volume conservation yield

$$
\psi = \psi_y = 0 \quad \text{at } y = -d,
\tag{2.3}
$$

$$
(\psi, \Omega)(x + L, y, t) \equiv (\psi, \Omega)(x, y, t), \quad f(x + L, t) \equiv f(x, t), \quad \int_0^L f\,\mathrm{d}x = 0.
\tag{2.4}
$$

The resulting problem depends on the depth d, the length L, the forcing amplitude a, the gravitational parameter $\mathscr{G}$, and the surface tension parameter $\mathscr{S}$, defined as

$$
(d, L, a) = \left(\frac{\omega^*}{\nu}\right)^{1/2}(d^*, L^*, a^*), \quad \mathscr{G} = \frac{g}{(\nu\omega^{*3})^{1/2}}, \quad \mathscr{S} = \frac{\sigma}{\rho(\nu^3\omega^*)^{1/2}},
\tag{2.5}
$$

where g is the acceleration due to gravity, σ is the surface tension, and ρ is the density. We shall perform a long-wave weakly nonlinear analysis, which requires that the aspect ratio be large and the forcing amplitude be appropriately close to its threshold value a_c, namely

$$
L \gg d, \quad k_c L \gg 1, \quad |a - a_c| \ll a_c,
\tag{2.6}
$$

where a_c and k_c are calculated from the problem obtained upon linearization in (2.1)–(2.4) around the quiescent flat state $\Omega \equiv \psi \equiv 0$, $f \equiv 0$. If we seek normal modes of the form $(\psi, \Omega, f) = (\psi_0(y, t), \Omega_0(y, t), f_0(t))\mathrm{e}^{\mathrm{i}kx}$, with $k \gg L^{-1}$, then we obtain

$$
\psi_{0yy} - k^2\psi_0 = \Omega_0, \quad \Omega_{0t} = \Omega_{0yy} - k^2\Omega_0 \quad \text{in } -d < y < 0,
\tag{2.7}
$$

$$
\left.
\begin{aligned}
&\mathrm{i}k(\mathscr{G} + \mathscr{S}k^2)f_0 - \psi_{0yt} - 4\mathrm{i}akf_0\cos 2t - 3k^2\psi_{0y} + \psi_{0yyy} = 0, \\
&f_{0t} - \mathrm{i}k\psi_0 = \psi_{0yy} + k^2\psi_0 = 0 \quad \text{at } y = 0,
\end{aligned}
\right\}
\tag{2.8}
$$

$$
\psi_0 = \psi_{0y} = 0 \quad \text{at } y = -d.
\tag{2.9}
$$

The marginal modes (non-trivial periodic solutions) are calculated by a numerically cheap method (Kumar & Tuckerman 1994). These solutions exist only along some marginal instability curves, a vs. k, such as those plotted in figure 2(a), which correspond to a Floquet multiplier equal to either 1 (labelled harmonic, H) or -1 (subharmonic, S). Since instability sets in above the marginal instability curves, the absolute minimum of these curves yields the *amplitude instability threshold in infinite domains*, a_c, attained at a wavenumber k_c. A plot of a_c vs. d^2 for the indicated values of $\mathscr{G}d^3$ and $\mathscr{S}d$ (which are independent of the forcing frequency) is given in figure 2(b). Assuming that d is not too small, which would require a large forcing amplitude (figure 2b, see also Mancebo & Vega 2002), the first instability is subharmonic and the eigenfunctions of (2.7)–(2.9) are such that

$$
(\psi_0, \Omega_0)(y, t + \pi) \equiv -(\psi_0, \Omega_0)(y, t), \quad f_0(t + \pi) \equiv -f_0(t);
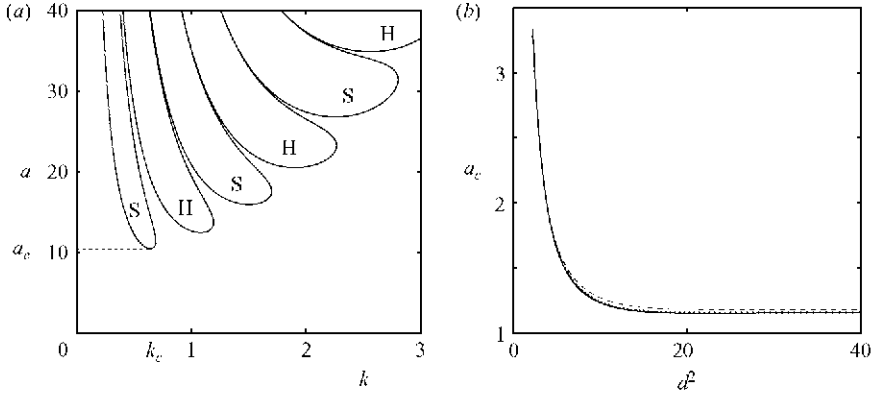\tag{2.10}
$$

FIGURE 2. Linear stability of the flat state in shallow containers for subharmonic (S) and harmonic (H) modes, as calculated by Mancebo & Vega (2002). (a) Marginal instability curves of (2.7) (2.9) for $\mathscr{G} = \mathscr{S} = d = 1$. (b) The instability threshold, $a_c \equiv a_c^*(\omega^*/\nu)^{1/2}$ vs. $d^2 \equiv d^{*2}\omega^*/\nu$ for the following values of $\mathscr{G}d^3 \equiv gd^{*3}/\nu$ and $\mathscr{S}d \equiv \sigma d^*/(\rho\nu^2)$: $\mathscr{G}d^3 = \mathscr{S}d = 1$ (——); $(\mathscr{G}d^3, \mathscr{S}d) = (1, 0)$ (– – –); $(\mathscr{G}d^3, \mathscr{S}d) = (0, 1)$ (· · ·).

thus $(\psi_0, \Omega_0)(y, t + 2\pi) \equiv (\psi_0, \Omega_0)(y, t)$, $f_0(t + 2\pi) \equiv f_0(t)$, and

$$\langle\psi_0\rangle^t \equiv \langle\Omega_0\rangle^t \equiv \langle f_0\rangle^t \equiv 0, \tag{2.11}$$

where the temporal mean value $\langle\cdot\rangle^t$ is defined as

$$\langle g\rangle^t = \frac{1}{2\pi}\int_0^{2\pi} g(t)\,\mathrm{d}t. \tag{2.12}$$

Also, the eigenfunctions can be selected such that

$$\mathrm{i}\psi_0, \quad \mathrm{i}\Omega_0, \quad f_0 \quad \text{are real}, \tag{2.13}$$

which means that the mode is a standing wave (SW).

In addition to these SWs, we have a mean flow that is associated with the long-wave deformational modes. These exhibit the dispersion relation $\lambda = -\mathscr{G}d^3k^2/3 + O(k^4)$, as $k \to 0$. Thus, they are nearly marginal in large domains (λ is small for small k), and must be also considered.

3. Low-frequency or shallow layer: $k_c d \sim 1$

Here, we consider the *distinguished limit* $k_c \sim d \sim \mathscr{G} \sim \mathscr{S} \sim 1$, $|a - a_c| \sim L^{-2} \ll 1$, in which we are anticipating the convenient relation between $a - a_c$ and L in order that as many terms as possible are of the same order in (3.3) below. We introduce the rescaled bifurcation parameter Σ and the slow space and time variables ξ and T,

$$\Sigma = L^2(a - a_c), \quad \xi = L^{-1}x, \quad T = L^{-2}t, \tag{3.1}$$

and seek the following expansions in powers of the small parameter L^{-1}

$$(\psi, \Omega, f) = L^{-1}A(\xi, T)(\psi_0, \Omega_0, f_0)\mathrm{e}^{\mathrm{i}k_c x} + \text{c.c.} + \dots$$
$$+ (L^{-3}\psi^m(\xi, y, T), L^{-3}\Omega^m(\xi, y, T), L^{-2}f^m(\xi, T)) + \dots, \tag{3.2}$$

where c.c. stands hereinafter for the complex conjugate and only the leading-order terms associated with the surface waves and the mean flow are displayed (cf. (A 3) in

Appendix A). It turns out that the mean flow is slaved to the free-surface elevation it produces. (ψ_0, Ω_0, f_0) and k_c are as defined in §2 and the complex amplitude of the surface waves, A, and the mean flow variables, ψ^m, Ω^m and f^m, are independent of the short space and time variables x and t (which means that they are slowly varying in both space and time), and governed by the following coupled amplitude–mean flow (CAMF) equations, which are derived in Appendix A,

$$A_T = \alpha_1 A_{\xi\xi} + \alpha_2 \Sigma A + \alpha_3 A |A|^2 + \alpha_4 f^m A, \quad f_T^m = \frac{\mathscr{G}d^3}{3} f_{\xi\xi}^m + \beta_1 (|A|^2)_{\xi\xi}. \quad (3.3a,b)$$

The various terms on the right-hand side of (3.3a) account for sideband diffusion, departure from the threshold, standard cubic nonlinearity and coupling to the mean flow; additional terms depending on the derivatives of ψ^m are higher order if d is bounded (but see Appendix B). The two terms on the right-hand side of (3.3b) account for the restoring effect of gravity and coupling to the surface waves. The boundary conditions,

$$A(\xi + 1, T) \equiv e^{i\delta} A(\xi, T), \quad f^m(\xi + 1, T) = f^m(\xi, T), \quad \int_0^1 f^m \, d\xi = 0, \quad (3.4)$$

result from (2.4) and the spatial detuning δ is the mismatch between the basic wavelength and the length of the domain, namely

$$\delta = k_c L \pmod{2\pi} \quad \text{with} \ -\pi < \delta \leqslant \pi. \quad (3.5)$$

The coefficients $\alpha_1, \ldots, \alpha_4$, and β_1 are all real (as could have been anticipated from invariance under the action $A \to \bar{A} = $ complex conjugate of A, which results from horizontal reflection), and are plotted vs. d^2 in figure 3 for the indicated values of $\mathscr{G}d^3$ and $\mathscr{S}d$. No comparison is possible with previous analyses in the literature because these coefficients (in particular, α_3 and β_1) have not been calculated before. Note that α_1 and α_2 are both positive; α_3 exhibits both signs, and is negative for large d; when it is positive (roughly, for $d^2 < 7$ in figure 3), the dynamics are subcritical, namely the solution either converges to the trivial state $A = f^m = 0$ (when this is stable and initial conditions are sufficiently small), or diverges for large time. Thus, interesting dynamics can only occur if $\alpha_3 < 0$, as we assume hereinafter. The term α_4 also exhibits both signs and β_1 is negative.

Considering the generic case in which all coefficients in (3.3) are non-zero, we introduce the new variables defined as

$$B = \left(-\frac{\alpha_3}{\alpha_1} \right)^{1/2} A, \quad \phi_\xi = -\frac{\alpha_4}{\alpha_1} f^m, \quad \tau = \alpha_1 T, \quad (3.6)$$

to rewrite (3.3) and (3.4) as

$$B_\tau = B_{\xi\xi} + \mu B - B |B|^2 - \phi_\xi B, \quad \phi_\tau = \gamma_1 \phi_{\xi\xi} - \gamma_2 (|B|^2)_\xi, \quad (3.7a,b)$$

$$B(\xi + 1, \tau) = e^{i\delta} B(\xi, \tau), \quad \phi(\xi + 1, \tau) = \phi(\xi, \tau), \quad \int_0^1 \phi(\xi, \tau) \, d\xi = 0, \quad (3.8)$$

where the last integral condition is imposed only to avoid the spurious symmetry $\phi \to \phi + \text{constant}$, δ is still as defined in (3.5), and

$$\mu = \frac{\alpha_2 \Sigma}{\alpha_1}, \qquad \gamma_1 = \frac{\mathscr{G}d^3}{3\alpha_1}, \qquad \gamma_2 = -\frac{\alpha_4 \beta_1}{\alpha_1 \alpha_3}. \quad (3.9)$$
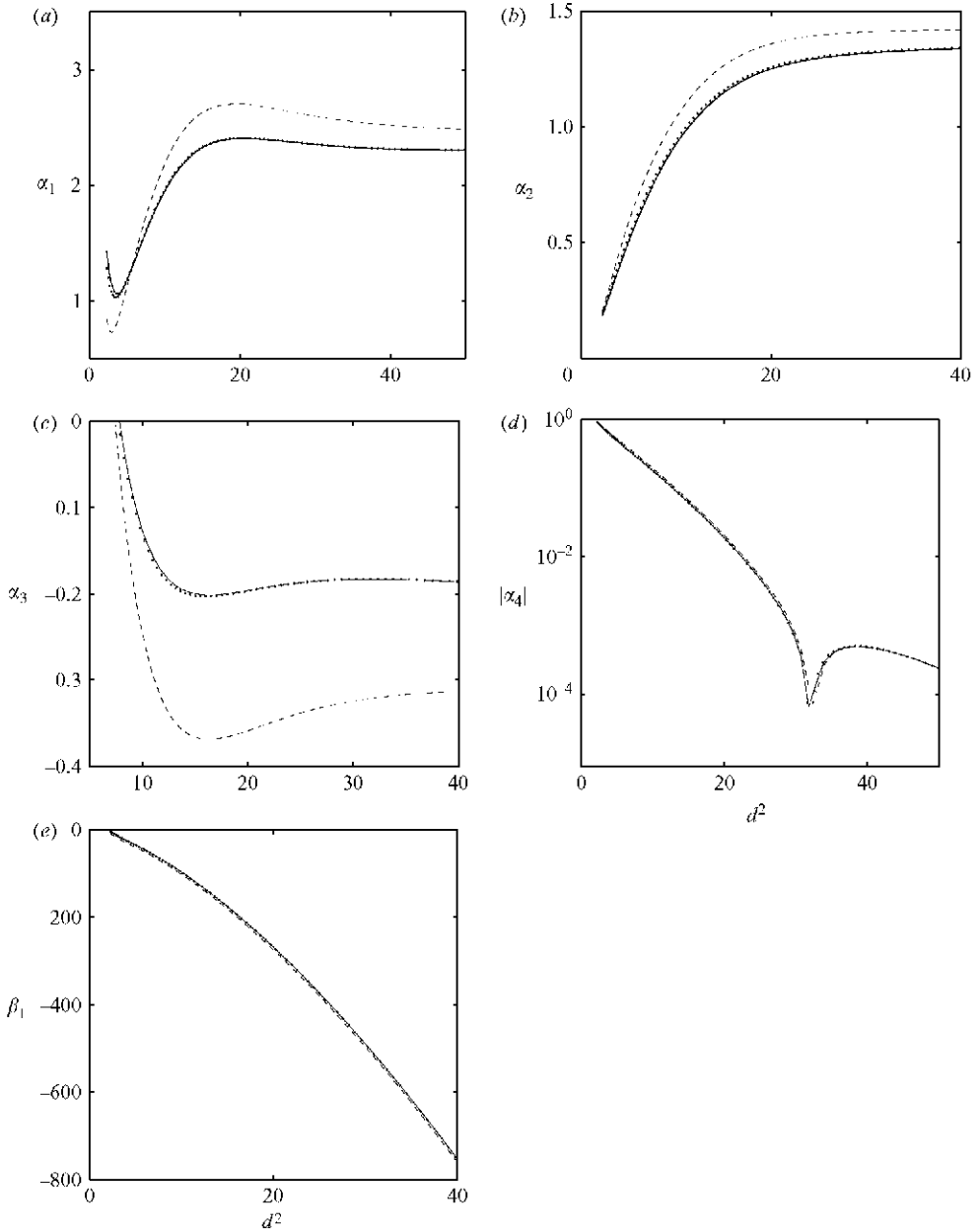
FIGURE 3. The coefficients $\alpha_1, \ldots, \alpha_4$ and β_1 appearing in (3.3) in terms of d^2 for the values of $\mathcal{G}d^3$ and $\mathcal{S}d$ indicated in the caption of figure 2; in the semilogarithmic plot (d), α_4 changes sign at $d^2 \simeq 32.3$ and is positive on the left-hand side.

Note (figure 4) that $\gamma_1 > 0$, but γ_2 is negative and fairly large for $d^2 \sim 1$, and positive and small for large d^2; the change of sign at $d^2 \simeq 32.3$ is due to the change of sign of α_4.

The rescaled CAMF equations (3.7) have been obtained using symmetry arguments by Coullet & Iooss (1990) in their analysis of spatially periodic patterns, and by Matthews & Cox (2000) in their study of a system with a conservation law that
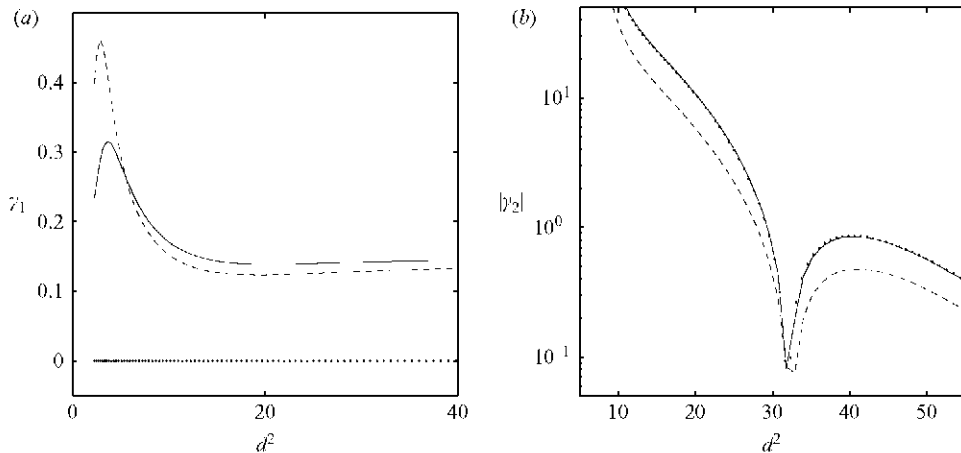
FIGURE 4. The coefficients of (3.7), γ_1 and $\gamma_2|$ (γ_2 vanishes at $d^2 \sim 32.3$, and is positive to the right-hand side of this value) in terms of d^2 for the values of $\mathscr{G}d^3$ and $\mathscr{S}d$ indicated in the caption of figure 2. Only the part of these curves corresponding to negative values of α_3 is considered.

is invariant under the $O(2)$ group generated by reflection and translations. We also have invariance under $O(2)$ and the free-surface elevation is a conserved quantity because of volume conservation (the second boundary condition (2.2) can be written as $f_t = [\psi(x, f(x,t),t)]_x$). For this reason (3.7) (3.8) are also obtained in large-aspect-ratio viscous fluid systems with a free surface, when a stationary (or a SW) mode with a non-zero wavenumber is destabilized, as in Bénard–Marangoni convection (Golovin, Nepomnyashchy & Pismen 1994).

Equations (3.7)–(3.8) are invariant under the four actions

$$\xi \rightarrow -\xi, \quad \phi \rightarrow -\phi; \quad B \rightarrow B; \quad \xi \rightarrow \xi + c_1; \quad B \rightarrow \mathrm{e}^{\mathrm{i}c_2} B,$$

for arbitrary constants c_1 and c_2, which result from the invariance of the original problem (2.1)–(2.4) under $O(2)$, but generate a larger symmetry group. The additional symmetries are an artefact of truncation and need not be present at higher order. Thus they must be interpreted with care (Knobloch 1995).

The simplest steady states of (3.7)–(3.8) ($|B| = $ constant) correspond to spatially uniform SWs, which are in branches that bifurcate from the trivial state at $\mu = \delta_n^2$, with $\delta_n = \delta + 2n\pi$ for $n = 0, \pm1, \pm2, \ldots$. The linear stability of these is analysed in Appendix C and illustrated in figure 5. At the secondary instability points, which can be either stationary or oscillatory (Appendix C), new branches of steady or periodic solutions appear that are no longer spatially uniform. Further stability properties of non-uniform steady states have been analysed by Norbury, Wei & Winter (2002) (in the limit $|\mu| \gg 1$ and the restricted case $\delta = 0$, $B = $ real) and by Vega (2005) in the general case. Summarizing these results, the system exhibits a Lyapunov function if $\gamma_2 \leqslant 0$, which means that all bounded solutions converge to steady states for large time. In fact, all solutions are bounded if $\gamma_1 + \gamma_2 \geqslant 0$. If instead $\gamma_1 + \gamma_2 < 0$, then some solutions diverge at finite time and most steady states with non-constant amplitude are unstable (Vega 2005), but the system also exhibits non-uniform steady states that are exponentially stable (Norbury et $al.$ 2002). Note (figure 4) that all these cases occur in practice.
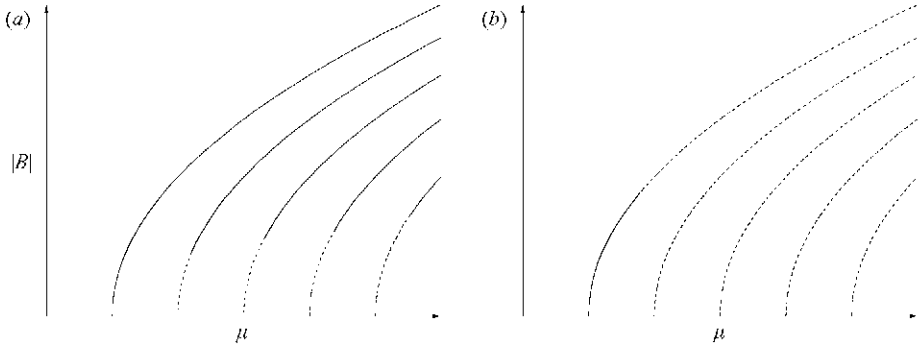
FIGURE 5. Stable (——) and unstable (· · · ·) uniform steady states of (3.7) (3.8), which correspond to SWs with spatially constant amplitude (called spatially uniform SWs along the paper) of the system, for: (a) $\gamma_1 + \gamma_2 > 0$ and (b) $\gamma_1 + \gamma_2 < 0$; all instabilities are stationary if $\gamma_2 < 0$, but some of them can be oscillatory if $\gamma_2 > 0$. (a) also applies to the amplitude equation (3.12) with $\Gamma > -1$.
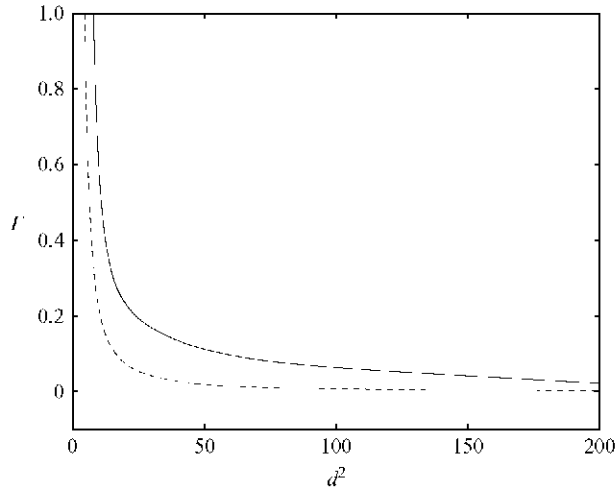

FIGURE 6. The coefficient Γ appearing in (3.12) vs. $d^2 = d'^2\omega^*/\nu$ for $\mathcal{G}/d \equiv g/(d^*\omega^{*2}) = 3.5$ and $\mathcal{S}/d^3 \equiv \sigma/(\rho d^{*3}\omega^{*2}) = 0$ (· · · ·) and 0.5 (——). As in figure 4, we are only plotting that part of the curve corresponding to negative values of α_3.

3.1. The limit of small viscosity: $\mathcal{G} \gg 1$, $\mathcal{S} \gg 1$, $k_c d \sim 1$

Using the estimates (A 36), (A 38), (A 39) and (A 40) in Appendix A, we obtain that as either $\mathcal{G} \gg 1$ or $\mathcal{S} \gg 1$ viscous effects are weak and $\varepsilon = k_c^2 \ll 1$; if in addition $d \sim k_c^{-1} \gg 1$, then depth is comparable to wavelength, and the container is not deep (cf. §4.1). Using the definition (3.9), we obtain readily that $\gamma_1 \sim |\gamma_2| \sim \varepsilon^{-1/2} \gg 1$. Thus, the two terms on the right-hand side of (3.7b) are both large and two time scales appear in (3.7) (3.9). In a short time scale $\tau \sim d^{-2}$, the free-surface elevation approaches the pseudo-steady-state

$$\phi_\xi = \Gamma(|B|^2 - \langle |B|^2 \rangle^\xi), \tag{3.10}$$

where the spatial mean value $\langle \cdot \rangle^\xi$ and the parameter Γ (plotted in figure 6) are

defined as

$$\langle |B|^2 \rangle^\xi = \int_0^1 |B|^2 \, d\xi, \quad \Gamma = \frac{\gamma_2}{\gamma_1} \equiv \frac{-3\alpha_4\beta_1}{\alpha_3 \mathscr{G} d^3}. \tag{3.11}$$

Substituting (3.10) into (3.7a), we obtain the following non-local Ginzburg–Landau (NLGL) equation for the evolution of B in the time scale $\tau \sim 1$

$$B_\tau = B_{\xi\xi} + \mu B - (1 + \Gamma)|B|^2 B + \Gamma \langle |B|^2 \rangle^\xi B, \quad B(\xi + 1, \tau) \equiv e^{i\delta} B(\xi, \tau). \tag{3.12}$$

The non-local term is due to the mean flow and thus has never appeared in previous analyses of Faraday waves. This is a particular case of a more general NLGL equation that exhibits complex coefficients and applies in a variety of contexts (Martel & Vega 1996 and references therein). The NLGL equation (3.12) also appears with real coefficients from the outset in the analysis of steady bifurcations of systems involving non-local terms (e.g. ferromagnetic resonance or current instability, Elmer 1988).

The simplest steady states of (3.12) with constant $|B|$ (SWs) and their linear stability have been analysed (Elmer 1988); see also Appendix C, where it is seen that the bifurcation diagram in figure 5(a) applies. More general SWs have been considered by Norbury et al. (2002) (restricted case $\delta = 0$, $B = $ real, and $|\mu| \gg 1$) and Vega (2005) (general case). Vega, in particular, shows that all SWs with non-constant $|B|$ are unstable if $\Gamma \geqslant 0$, which is precisely the case for viscous Faraday waves (see figure 6). Since, in addition, the NLGL equation (4.4) exhibits a Lyapunov function, the large-time dynamics are dominated by the stable spatially uniform SWs.

4. High-frequency or deep layer: $k_c d \gg 1$

We now assume that $k_c \sim 1$ and $d \gg 1$. As explained in Appendix A,

$$\alpha_4 \to 0 \quad \text{exponentially as} \quad k_c d \to \infty. \tag{4.1}$$

Thus, in principle, the surface waves become decoupled from the mean flow in deep containers. However, as explained in Appendix B, the mean flow produces a new term (which is negligible for bounded $k_c d$) in the amplitude equation, which becomes a non-potential Ginzburg–Landau (NPGL) equation, namely (B6) in Appendix B, which is

$$A_T = \alpha_1 A_{\xi\xi} + \alpha_2 \Sigma A + \alpha_3 A|A|^2 + i\frac{\alpha_6\alpha_8 d}{4L}(|A|^2)_\xi A, \tag{4.2}$$

where α_1, α_2 and α_3 are as calculated in Appendix A (with $d = \infty$) and α_6 and α_8 are as calculated in Appendix B. All these are plotted in figure 7 after convenient rescaling (invoking (A36) and (A39)) to obtain $O(1)$-quantities as viscosity goes to zero. In the distinguished limit

$$|a - a_c| \sim L^{-2}, \quad \left| \frac{\alpha_3}{\alpha_6\alpha_8} \right| \sim \frac{d}{L} = D \ll 1, \tag{4.3}$$

(4.2) can be rescaled in terms of the variable B defined in (3.6), as

$$B_\tau = B_{\xi\xi} + \mu B - B|B|^2 + i\gamma D(|B|^2)_\xi B, \quad B(\xi + 1, \tau) \equiv e^{i\delta} B(\xi, \tau), \tag{4.4}$$

where the boundary condition results from the periodicity of the domain, $\gamma D \sim 1$, and
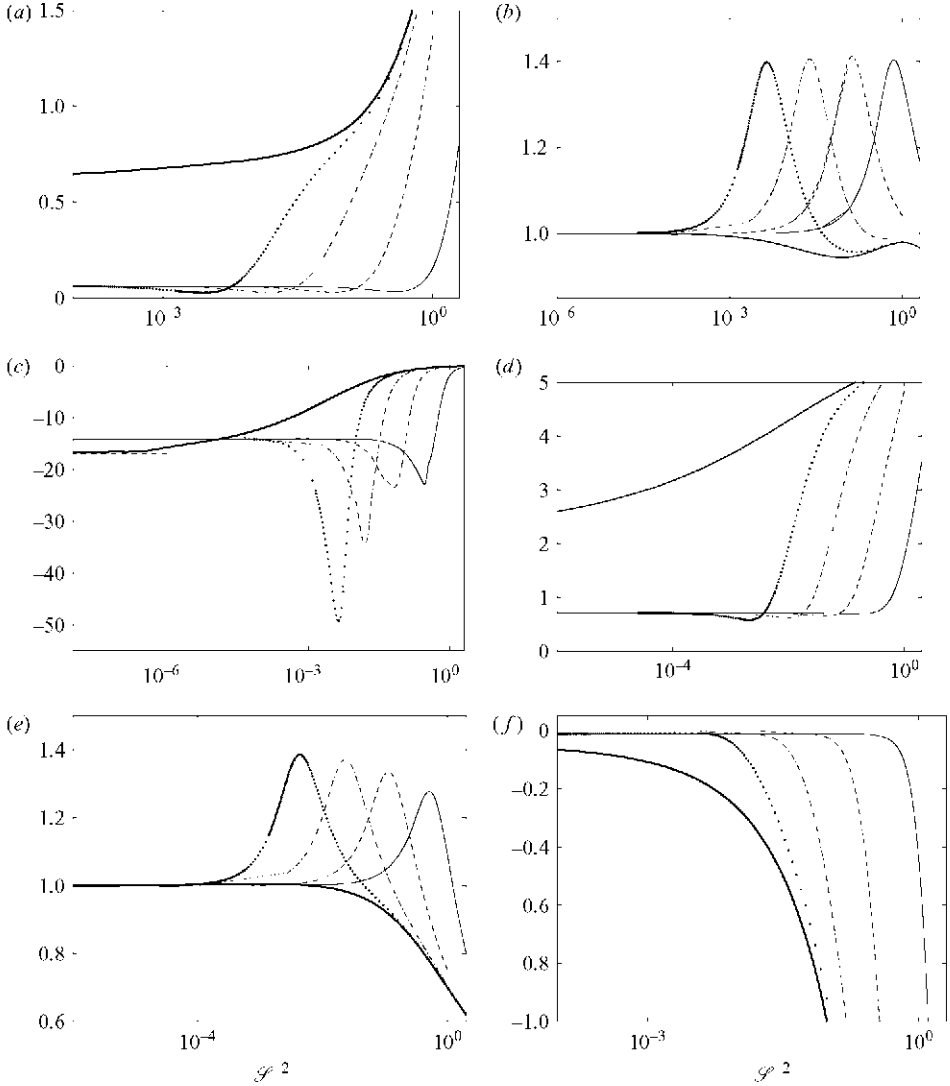
$$\gamma = \frac{\alpha_6\alpha_8}{4\alpha_3}. \tag{4.5}$$

FIGURE 7. The various coefficients in (4.2) and (4.4) rescaled with $\mathscr{G}$ and $\mathscr{S}$ (according to (4.8), (A 39)–(A 40), and (B8)) as follows: (a) $(\mathscr{G} + \mathscr{S}^{1/3})^{-4}\alpha_1$, (b) $(\mathscr{G} + \mathscr{S}^{1/3})\alpha_2$, (c) $(\mathscr{G} + \mathscr{S}^{1/3})^4\alpha_3$, (d) $(\mathscr{G} + \mathscr{S}^{1/3})^{-2}\alpha_6$, (e) $(\mathscr{G} + \mathscr{S}^{1/3})\alpha_8$, and (f) $(\mathscr{G} + \mathscr{S}^{1/3})^{-5}\gamma$, in terms of $\mathscr{S}^{-2} \equiv \rho^2 v^3 \omega^* / \sigma^2$ for fixed values of $\mathscr{G}/\mathscr{S}^3 \equiv \rho^3 g v^4 / \sigma^3$: 0 (———), $10^{-3}(\cdots)$, 10^{-2} (·), 10^{-1} (   ), and 1 (   ).

The coefficient γ is plotted in figure 7(f). Note that it is always negative and that $|\gamma| \gg 1$ as assumed provided that $\mathscr{G} + \mathscr{S}^{1/3}$ is (even moderately) large; see §4.1. The NPGL equation (4.4) differs from the standard Ginzburg–Landau (GL) equation with real coefficients only in the last term appearing in the right-hand side. This term does affect qualitatively the dynamics because it (i) prevents the existence of a Lyapunov function (thus the bounded solutions need not converge to steady states for large time), and (ii) breaks a spurious reflection symmetry because the equation is only invariant under the actions

$$\xi \to -\xi, \quad B \to \bar{B}; \quad \xi \to \xi + c_1; \quad B \to e^{ic_2}B, \tag{4.6}$$
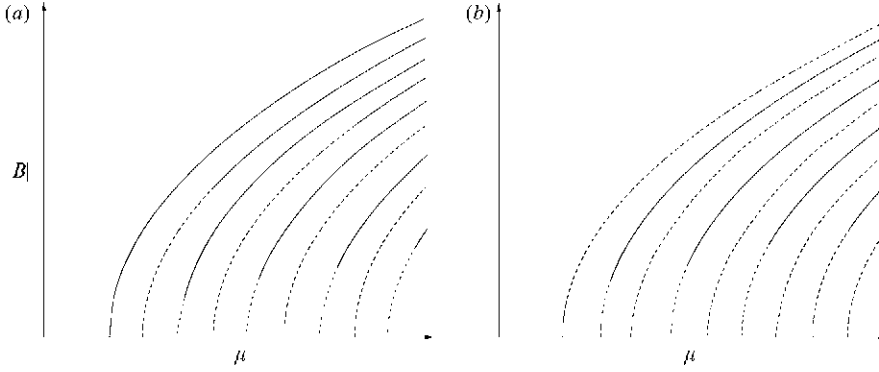
FIGURE 8. Stable (———) and unstable (- - -) spatially uniform SWs of (4.4) for (a) $2\gamma D\delta > 1$ and (b) $2\gamma D\delta < 1$.

while the real GL equation is invariant under $\xi \to -\xi$ and $B \to \bar{B}$ separately. One of these symmetries is spurious because the original problem exhibits only one reflection symmetry, namely $x \to -x$. Also, all solutions of the NPGL equation are bounded as $\tau \to \infty$, as seen from the exact relation

$$\frac{1}{2}\frac{\mathrm{d}}{\mathrm{d}\tau}\langle |B|^2\rangle^\xi = -\langle|B_\xi|^2\rangle^\xi + \mu\langle|B|^2\rangle^\xi - \langle|B|^4\rangle^\xi,$$

where $\langle\cdot\rangle^\xi$ is defined in (3.11). This relation is obtained multiplying (4.4) by B, taking the real part, and proceeding as usual. The uniform steady states of (4.4) correspond again to spatially uniform SWs and are of the form $B = B_n = \sqrt{\mu - \delta_n^2}\exp\mathrm{i}\delta_n\xi$, with $\delta_n = \delta + 2\pi n$, for $n = 0, \pm1, \pm2, \dots$. The linear stability of these is analysed in Appendix C and illustrated in figure 8. Note that:

(i) If $2\gamma D\delta \leqslant 1$, then the whole first branch $(n=0)$ is stable and the remaining branches are stable if $2\gamma D\delta_n < 1$ and $R_n > 2\sqrt{(\delta_n^2 - \pi^2)/(1 - 2\gamma D\delta_n)}$ and are unstable otherwise.

(ii) If $2\gamma D\delta > 1$, then the first branch is stable if $0 < R_0 < 2\sqrt{(\pi^2 - \delta^2)/(2\gamma D\delta - 1)}$ and unstable otherwise. The remaining solutions are unstable if either $n > 0$ or if $n < 0$ and $R_n < 2\sqrt{(\pi^2 - \delta^2)/(2\gamma D\delta - 1)}$ and stable otherwise. Note that if $0 < \delta < \pi$ and γD is sufficiently large, then the first branch is stable only in the close vicinity of the threshold and there are values of μ such that no spatially uniform SW is stable, meaning that the large-time dynamics must involve more complex states (at least, spatially modulated SWs).

4.1. Small-viscosity limit: $\mathcal{G} \gg 1$, $\mathcal{S} \gg 1$, $k_c d \gg 1$

As explained in Appendix A, either $\mathcal{G}$ or $\mathcal{S}^{1/3}$ is large in this limit. Since we have now a deep layer, $k_c d \gg 1$, the inviscid dispersion (A 37) relation simplifies to

$$k_{0c}\left(\mathcal{G} + k_{0c}^2\mathcal{S}\right) = 1. \tag{4.7}$$

Thus, $k_c \simeq k_{0c} \sim (\mathcal{G} + \mathcal{S}^{1/3})^{-1} \ll 1$. In order to compare with nearly inviscid analyses in the literature, we use the parameters defined in (A 38), namely

$$S = \frac{k_{0c}^2\mathcal{S}}{k_{0c}^2\mathcal{S} + \mathcal{G}} \sim 1, \quad \varepsilon = k_{0c}^2 \sim \frac{1}{\left(\mathcal{G} + \mathcal{S}^{1/3}\right)^2} \ll 1. \tag{4.8}$$

According to the estimates (A 39) and (B 8) in Appendixes A and B,

$$\tilde{\beta}_1 = \frac{\alpha_6 \alpha_8 \varepsilon^{1/2}}{4} \sim 1, \quad \tilde{\beta}_2 = \frac{\alpha_3}{\varepsilon^2} \sim 1, \tag{4.9}$$

which means that the coefficients γ and D can be replaced by

$$\tilde{\gamma} = \frac{\tilde{\beta}_1}{\tilde{\beta}_2} \sim 1, \quad \tilde{D} = \frac{D}{\varepsilon^{5/2}} \sim 1 \tag{4.10}$$

in (4.5), which is rewritten here for convenience,

$$B_\tau = B_{\xi\xi} + \mu B - B|B|^2 + i\tilde{\gamma}\tilde{D}(|B|^2)_\xi B, \quad B(\xi+1,\tau) \equiv e^{i\delta} B(\xi,\tau). \tag{4.11}$$

Note that $\tilde{\beta}_1$ accounts for the effect of the mean flow, but $\tilde{\beta}_2$ is just a rescaled version of the cubic coefficient α_3. Now we check the asymptotic values of these two quantities calculated in the literature.

The mean flow has been considered only by Mancebo & Vega (2004), who calculated the following asymptotic expression

$$\tilde{\beta}_1 \simeq \frac{1+2S}{2}. \tag{4.12}$$

This approximation is compared with its exact value calculated above in figure 9(a). Note that the agreement is quite good for $\varepsilon < 0.005$.

Comparison of the rescaled cubic coefficient $\tilde{\beta}_2$ shows quite good agreement with the exact calculation by Chen & Viñals (1999) for $\varepsilon = 10^{-4}$, but $O(1)$ discrepancies with all asymptotic results in the literature (figure 9b) because (i) $\tilde{\beta}_2$ shows a extreme sensitivity on wavenumber at low viscosity, and (ii) all asymptotic calculations of $\tilde{\beta}_2$ in the literature have been made at the inviscid value of k_c, k_{c0}. These two points have been explained in a careful asymptotic analysis by Mancebo & Vega (2004), who showed that the above-mentioned wavenumber shift, $k_c - k_{c0}$, has an $O(1)$ effect on $\tilde{\beta}_2$. In order to illustrate that, we calculate the cubic coefficient $\tilde{\beta}_2$ using the exact expression (A 23) (with $j=3$ and $d=\infty$) at (a) $k=k_c$ and (b) at $k=k_{c0}$; the latter is denoted as $\tilde{\beta}_{20}$. The difference between both is labelled $\tilde{\beta}_{21}$ and is plotted vs. S in figure 9(c) for the indicated values of ε, together with the following asymptotic approximation as $\varepsilon \to 0$ calculated by Mancebo & Vega (2004)

$$-\tilde{\beta}_{21} = \frac{4}{1+2S} \left(\frac{2}{1+3S} - \frac{3S}{1-3S} + \frac{9S}{4} \right). \tag{4.13}$$

Note that the agreement is quite good. These results open the question of whether the former approximations in the literature (which ignored the wavenumber shift) could approximate well the cubic coefficient calculated at k_{c0}. The answer is again no, as shown in figure 9(d). Thus there must be additional mistakes in former calculations, which cannot be safely used, and we do not have an asymptotic result available for $\tilde{\beta}_{20}$. However, the exact calculation plotted in figure 9(b) for quite small ε can be taken as a safe mark for any asymptotic calculation; note that the associated value of $\tilde{\beta}_2$ has been checked against independent calculations by Chen & Viñals (1999). For completeness, we have obtained (by mean squares fit with the exact solution for $\varepsilon = 10^{-5}$, with a maximum relative error of 10^{-2}) the following empirical asymptotic expression for the rescaled cubic coefficient

$$-\tilde{\beta}_2 = -\frac{1}{30(1-3S)^2} + \frac{61S}{10(1-3S)^2} + \frac{4-9S}{3(1+2S)(1-9S^2)} + \frac{S}{10} + \frac{4}{9}. \tag{4.14}$$
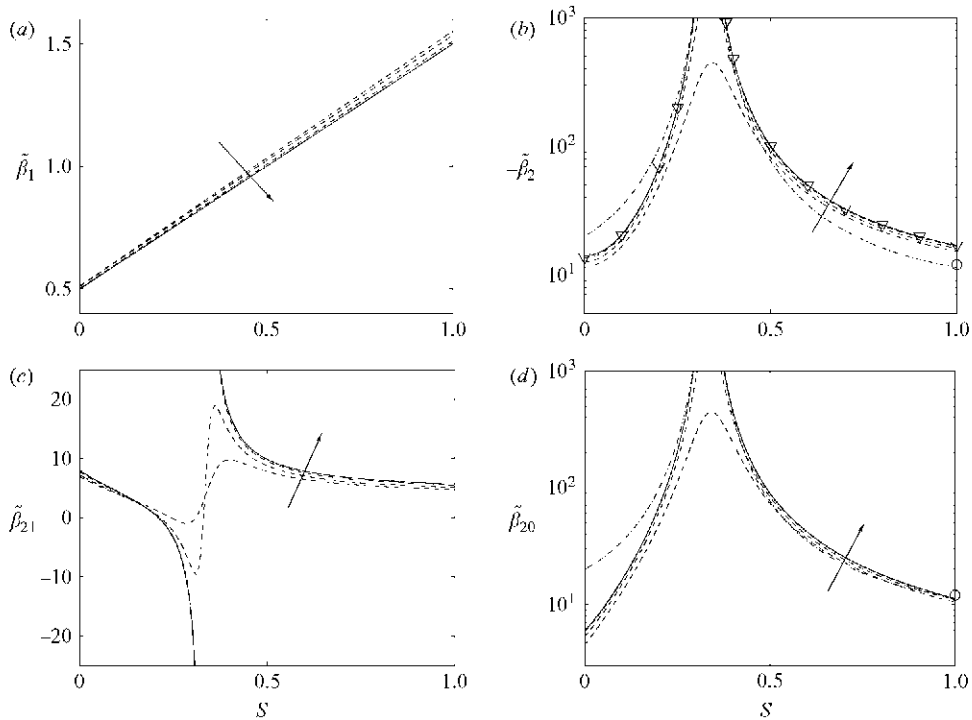
FIGURE 9. The nonlinear coefficients (a) $\tilde{\beta}_1$ and (b) $-\tilde{\beta}_2$ defined in (4.9); (c) the effect of the viscous wavenumber shift, $-\tilde{\beta}_{21}$; and (d) $-\tilde{\beta}_{20}=$ the value of $-\tilde{\beta}_2$ calculated at $k=k_{c0}$. ( ) as given by the asymptotic expressions (4.12), (4.14), (4.13) and (4.15), respectively; $(---)$ as calculated in this paper for $\varepsilon = 1.25 \times 10^{-2}$, 5×10^{-3}, 5×10^{-4}, and 10^{-4} (the arrows indicate decreasing values of ε); (·) as calculated by Zhang & Viñals (1997) for $\varepsilon \to 0$, and ($\bigcirc$) as calculated by Hansen & Almstrom (1997) for $\varepsilon \to 0$ and $S = 1$. The result for $\varepsilon = 10^{-4}$ in (b) is indistinguishable from the exact calculation by Chen & Viñals (1999) (∇), which has been kindly provided to us by Peilong Chen. In fact, the cubic coefficient calculated in this paper is eight times that calculated by Zhang & Viñals (1997), Hansen & Almstrom (1997), and Chen & Viñals (1999) owing to differences in the scaling of the eigenfunctions.

This expression has been plotted with a solid line in figure 9(b), and combined with (4.13) yields the following expression, which is plotted with a solid line in figure 9(d),

$$-\tilde{\beta}_{20} = -\tilde{\beta}_2 + \tilde{\beta}_{21}. \tag{4.15}$$

5. Concluding remarks

The amplitude equations derived above are all new in the context of Faraday waves. They have been obtained in various limiting cases:

1. For shallow containers, the relevant equations are the CAMF equations (3.3), whose coefficients are plotted in figure 3 in terms of the non-dimensional depth in the interval where the cubic coefficient α_3 is negative. For smaller values of d, α_3 is positive and the dynamics are subcritical. In the supercritical case, the amplitude equations are rewritten in the form (3.7) (3.8), with the coefficients γ_1 and γ_2 as plotted in figure 4. The simplest spatially uniform SWs are illustrated in the bifurcation diagrams in figure 5. As explained in § 3, depending on the signs of γ_2 and $\gamma_1 + \gamma_2$, the solutions of

the amplitude equations can either be bounded for large time or not, either converge to spatially uniform SWs for large time or not, and either possess asymptotically stable spatially modulated SWs or not. Note that if $\gamma_1 + \gamma_2 > 0$ (which occurs for large values of d^2 in figure 4), all spatially uniform SWs are unstable for large μ (figure 5b) and the system exhibits spatially modulated SWs that are stable; but in this case, the system also shows solutions that diverge for finite time. If $\gamma_1 + \gamma_2 < 0$, the system always exhibits spatially uniform SWs that are stable (figure 5b) and thus are *a priori* the best candidates for being observed at large time.

2. At small viscosity, the system (3.7) reduces to the NLGL equation (3.12), with the non-local coefficient $\Gamma > 0$ plotted in figure 6. As explained in §3.1, the bifurcation diagram is as that in figure 5(a) and all solutions converge to spatially uniform SWs for large time.

3. In deep containers and significant viscous effects, the coefficient γ_2 (accounting for coupling to the mean flow) in (3.7) converges to zero. However, since depth is large, the mean flow is stronger and a new coupling effect comes into play that leads to the NPGL equation (4.2) (or its rescaled version (4.4)). This equation contains a non-potential term (namely, the last term in (4.2) or (4.4)) that is small (recall that $D = d/L \ll 1$) unless $|\gamma| \gg 1$, which occurs for (even moderately) small viscosity. This term breaks a spurious symmetry and prevents the existence of a Lyapunov function. Thus, the dynamics are expected to be richer in this case. The spatially uniform SWs and their linear stability are analysed in Appendix C, and illustrated in figure 8. As explained in §4, if $0 < \delta < \pi$ and γD is large (which is easily attained if viscosity is really small, see §4.1), then there are values of μ such that no spatially uniform SW is stable, suggesting that the large-time dynamics must include more complex attractors that spatially uniform SWs.

4. At quite small viscosity, the coefficient γ is large and a new scaling applies (see (4.11)). According to (4.9)–(4.10), the rescaled coefficient $\tilde{\gamma}$ depends on the coefficients α_6 and α_8 (which are associated with the mean flow) and on the cubic coefficient α_3. The product of α_6 and α_8 (in fact, its rescaled version, $\tilde{\beta}_1$, see (4.9)) is compared (with satisfactory results) in figure 9(a) with its rescaled asymptotic value for small viscosity calculated by Mancebo & Vega (2004); this is the only work in the literature where mean flows have been considered in connection with standing Faraday waves. The cubic coefficient α_3 instead has been calculated in various works, with controversial results, as noted by Hansen & Almstrom (1997), always for small viscosity and deep containers. Comparison with the exact results by Chen & Viñals (1999) is quite good, which was to be expected. Comparison with any other asymptotic results is bad because, as explained further by Mancebo & Vega (2004), all these results are incorrect. This is because all these analyses have ignored the effect of a shift of the wavenumber at the threshold owing to the interplay between viscous effects and parametric forcing; this shift has a $O(1)$ effect on the numerical value of the cubic coefficient. Comparison with the asymptotic expression for this wavenumber shift in Mancebo & Vega (2004) in figure 9(c), is quite good. Unfortunately, the correct calculation of the cubic coefficient at small viscosity is quite involved and outside the scope of this paper. In order to check any asymptotic calculation of this coefficient in the future, we give an expression (equation (4.14)), obtained by empirical fit with the exact results for $\varepsilon = 10^{-5}$, which is exact within $O(10^{-2})$-relative errors.

5. At small viscosity, the equations obtained above are correct immediately after the threshold. Further departure from the threshold leads to more general equations, which are derived and discussed by Mancebo & Vega (2004).

Experiment	ρ g cm^{-3}	ν cm^{2}s^{-1}	σ dyn cm^{-1}	d^* cm	$2\omega^*$ Hz	$\mathscr{G}$	$\mathscr{S}$	d	k_c
HW	0.9	4.3	10	6	50–110	0.233–0.072	0.096–0.095	36.5–54.1	0.64–0.65
E	1.22	1.02	67.6	0.29	51–100	0.476–0.174	4.06–3.05	3.67–5.12	0.56–0.62
B	0.84	0.25	26.2	1.0	54–137	0.845–0.220	18.82–12.02	26.4–41.3	0.34–0.43
KG	0.85	0.5	27	0.3	42 57	0.90 0.58	7.84 6.74	4.91 5.70	0.43 0.47
L	0.8	0.41	30	0.25	52 102	0.74 0.26	11.2 7.97	4.99 7.01	0.41 0.48
W	0.89	0.036	18.3	2	20 100	10.33 0.927	374 167	83.2 186	0.10 0.17

TABLE 1. The values of the non-dimensional parameters $\mathscr{G}$, $\mathscr{S}$ and d, and the non-dimensional wavenumber at the threshold for various experimental conditions in the literature: HW (Hoffmann & Wolf 1974); E (Edwards 1994; unpublished results that can be found in, e.g. Cerda & Tirapegui 1998); B (Bechhoefer *et al.* 1995); KG (Kudrolli & Gollub 1997); L (Lioubashevski, Fineberg & Tuckerman 1997); and W (Westra *et al.* 2003).

Experiment	γ_1	$-\gamma_2$	$-\gamma$	ε	S	$-\tilde{\gamma}$	AE
HW	$>10^3$	$<10^{-8}$	3.06–3.02	3.3–4.31	–	–	(4.4)
E	1.44–1.92	9.25–3.39	–	–	–	–	(3.7)
B	>100	$<10^{-4}$	18.2–13.9	0.11–0.18	–	–	(4.4)
KG	2.90–3.60	2.83–2.13	–	–	–	–	(3.7)
L	1.67–2.51	1.44–0.71	–	–	–	–	(3.7)
W	$>10^2$	$<10^{-6}$	194–255	0.0062–0.03	0.184–0.84	0.0061–0.038	(4.11)

TABLE 2. The various coefficients appearing in the amplitude equations (3.7), (3.7) and (4.11) for the experiments described in table 1. AE indicates the amplitude equation that applies to the experiment.

6. In order to have an idea of the scope of the equations derived above, we consider the values of the parameters $\mathscr{G}$, $\mathscr{S}$ and d, and the wavenumber at the threshold in the experimental conditions quoted in tables 1 and 2, which are discussed below.

(a) The container is shallow ($k_c d \sim 1$) and viscosity is significant ($\mathscr{G} + \mathscr{S} \sim 1$) in the experiments E, KG and L, in which the CAMF equations (3.7) apply. Note that $\gamma_1 \sim \gamma_2 \sim 1$ in KG and L, meaning that the mean flow and the cubic nonlinearity play similar roles in these cases, whereas $\gamma_1 \sim 1$ but $\gamma_2 \gg 1$ in E, meaning that the fundamental nonlinearity is provided by the mean flow in this case.

(b) The container is deep ($k_c d \gg 1$) and viscous effects are significant ($\mathscr{G} + \mathscr{S} \sim 1$) in HW and B, in which the NPGL equation (4.4) applies, with the coefficient γ as given in table 2. Note that $-\gamma$ is (at least somewhat) large in both cases, as assumed.

(c) The container is deep and viscosity is small in the experiment W. Thus, (4.11) applies, with $\tilde{\gamma}$ as indicated in table 2.

(d) As explained at the beginning of §2, if the two-dimensional model above is to be used as an approximation of an annular container, width must be small (say, one tenth) compared to length, but large (say, ten times) compared to depth. This imposes that $d/L = d^*/L^*$ be of the order of 0.01, which means that:

(i) L^* must be quite large, say 600 cm, in the experimental conditions HW.

(ii) $D = d/L$ is quite small in the experiments HW and B, meaning that the non-potential term in (4.4) is quite small. Thus this equation reduces to the standard Ginzburg–Landau equation with real coefficients in these two cases, which shows trivial dynamics.

(iii) In the experiment W instead $\tilde{\gamma}\tilde{D} \equiv \gamma D \sim 1$ and the role of the non-potential term is significant provided that $L^* \sim 200\,\mathrm{cm}$.

(iv) In the remaining experiments, in which (3.7) applies, $L^* \sim 100d^*$ takes reasonable values (ranging from 25 to 30 cm), and γ_2 is never small compared to γ_1. Thus the mean flow plays a significant role in these cases.

7. The cubic coefficient α_3 appearing in the unscaled amplitude equations (3.3) and (4.2) is negative in all experimental conditions in table 2 and also in the remaining experiments (which have also been checked but are not included in table 2 for the sake of brevity) by Hoffman & Wolf (1974), Bechhoefer et al. (1995), Kudrolli & Gollub (1997), Lioubashevski et al. (1997) and Westra et al. (2003). Positive values of α_3, which lead to a subcritical primary bifurcation never encountered experimentally, would require either a more viscous fluid, or a smaller depth (or a lower vibrating frequency). Some care must be taken when doing this because the primary instability need not be subharmonic as either ν is too large, or d^* is too small, or ω^* is too small (Mancebo & Vega 2002). Note that this subcritical transition appears when viscosity and depth effects are both significant; detuning instead plays no role. Thus this is of a completely different nature to the subcritical transition encountered at low viscosity for appropriate signs of detuning (Miles & Henderson 1990).

8. A physical explanation of this subcritical transition as the forcing frequency $\omega^* \to 0$ (which yields $d \to 0$, see (2.5)) follows noting that in this limit (a) time-derivatives are small (thus the solution follows a pseudo-steady state) and (b) effective 'gravity', $\tilde{g}(t^*) = g + 4a^*\omega^{*2}\cos 2\omega^* t^*$, points upwards in a part of the period, in which the Rayleigh–Taylor instability (Chandrasekhar 1961) comes into play. The simplest (non-flat) SWs of the system should approach a non-flat pseudo-steady state (associated with the Rayleigh–Taylor instability) in a part of the period and the flat state in the remaining part of the period. Thus, existence of non-flat SWs of the Faraday system should require existence of non-flat steady states of the Rayleigh–Taylor system with an effective gravity $\tilde{g}$. But the primary bifurcation from the flat state to non-flat steady states in the Rayleigh–Taylor system is subcritical (Lapuerta, Mancebo & Vega 2001 and references therein).

9. As indicated at the beginning of §2, the two-dimensional problem laterally unbounded layer considered in this paper should describe well, even quantitatively, Faraday waves in a three-dimensional annular container whose width is small compared to length, but large compared to depth. Of course, the one-dimensional Faraday waves considered above can only describe two-dimensional patterns in the three-dimensional container consisting of rolls oriented in the radial direction. Neither azimuthal rolls nor more complex patterns (e.g. squares, hexagons, quasi-patterns) can be described by the theory above. Note, that as shown by Zhang & Viñals (1997) and Chen & Viñals (1999), rolls (instead of squares, hexagons, etc.) are precisely the patterns that must be expected at large aspect ratio near the threshold provided that either viscosity is not too small (without further restrictions) or viscosity is small but capillary effects are sufficiently small compared to gravitational effects (namely, the parameter S defined in (4.8) is sufficiently small), and radial rolls are (perpendicular to the lateral boundaries and thus) the expected ones for generic initial conditions (see the various pictures involving rolls given by Kudrolli & Gollub 1997).

The analysis in this paper intends to provide a complete quantitative theory of one-dimensional standing Faraday waves in two-dimensional large-aspect-ratio containers. This is a first step to the analysis of three-dimensional large-aspect-ratio containers, which is lacking today. Current three-dimensional theory has always ignored both the mean flow (the only exception is the phenomenological model in Vega, Rüdiger &

Viñals 2003) and finite-depth effects (a toy model has been introduced for shallow containers by Westra *et al.* 2003) and thus this theory has been successful only in explaining the first bifurcation at threshold in deep containers (Westra *et al.* 2003). We hope that the analysis in this paper will stimulate further theoretical and experimental analyses of Faraday waves in large-aspect-ratio containers, with special emphasis on the mean flow, which is necessary to build a correct theory on the wave dynamics beyond threshold.

Appendix A. Derivation of the CAMF equations (3.3)

Here, we derive the CAMF equations (3.3) that apply in shallow containers, namely

$$A_T = \alpha_1 A_{\xi\xi} + \alpha_2 \Sigma A + \alpha_3 A|A|^2 + \alpha_4 f^m A, \quad f^m_T = \frac{\mathscr{G}d^3}{3} f^m_{\xi\xi} + \beta_1(|A|^2)_{\xi\xi}, \quad (A\,1a,b)$$

where Σ, ξ and T are as defined in (3.1), namely

$$\Sigma = L^2(a - a_c), \quad \xi = L^{-1}x, \quad T = L^{-2}t. \quad (A\,2)$$

To this end, we expand the solution in powers of the small parameter L^{-1}, as

$$
\begin{aligned}
(\psi, \Omega, f) = {}& L^{-1}A(\psi_0, \Omega_0, f_0)e^{ik_cx} + \text{c.c.} \\
&+ L^{-2}[iA_\xi(\psi_{11}, \Omega_{11}, f_{11})e^{ik_cx} + A^2(\psi_{12}, \Omega_{12}, f_{12})e^{2ik_cx} + \text{c.c.} + (0, 0, f^m)] \\
&+ L^{-3}[A_{\xi\xi}(\psi_1, \Omega_1, f_1) + \Sigma A(\psi_2, \Omega_2, f_2) + |A|^2A(\psi_3, \Omega_3, f_3) \\
&+ f^m A(\psi_4, \Omega_4, f_4)]e^{ik_cx} + \text{c.c.} + L^{-3}\left[(\psi^m, \Omega^m, f^m_1) + NRT\right] + \ldots, \quad (A\,3)
\end{aligned}
$$

where NRT denotes *non-resonant terms*, which either (*a*) depend on x as e^{imk_cx}, with $m \neq \pm 1$, or (*b*) are independent of x and exhibit a zero temporal mean. Here, we are anticipating the dependence of the various terms on the complex amplitude A and the variables associated with the mean flow. The analysis proceeds in a standard way, substituting (A 1)–(A 3) into (2.1)–(2.3), setting to zero the coefficients of L^{-1}, $L^{-2}, \ldots$, and applying solvability conditions to the various equations that provide resonant terms, which are either oscillatory (namely, proportional to $e^{\pm ik_cx}$) or slowly varying in x; the latter are associated with the mean flow. These two contributions are considered in §§ A.1 and A.2 below.

A.1. *Oscillatory terms: first amplitude equation (3.3)*

For convenience, we select the eigenfunction of (2.7)–(2.10), (ψ_0, Ω_0, f_0), such that

$$\frac{1}{\pi}\left|\int_0^\pi e^{-it}f_0(t)\,dt\right| = 1.$$

In order to apply solvability conditions, we consider the adjoint problem

$$\psi^*_{0yy} - k_c^2\psi^*_0 = \Omega^*_0, \quad -\Omega^*_{0t} = \Omega^*_{0yy} - k_c^2\Omega^*_0 \quad \text{in} \quad -d < y < 0, \quad (A\,4a,b)$$

$$ik_c(\mathscr{G} + \mathscr{S}k_c^2)f^*_0 + \psi^*_{0yt} - 4ia_ck_c\int^t f^*_{0t}(\tau)\cos 2\tau\,d\tau - 3k_c^2\psi^*_{0y} + \psi^*_{0yyy} = 0,$$

$$f^*_{0t} + ik_c\psi^*_0 = \psi^*_{0yy} + k_c^2\psi^*_0 = 0 \quad \text{at } y = 0, \quad (A\,5)$$

$$\psi_0^* = \psi_{0y}^* = 0 \quad \text{at } y = -d, \tag{A6}$$

where the operator $\int^t$ is defined as

$$\int^t g(\tau)\,d\tau = \int_{t_0}^t g(\tau)\,d\tau - \left\langle \int_{t_0}^t g(\tau)\,d\tau \right\rangle^t, \tag{A7}$$

with $\langle \cdot \rangle^t$ as defined in (2.12). The general solution to (A4)–(A6) is

$$(\psi_0^*(y,t),\,\Omega_0^*(y,t),\,f_0^*(t)) = C \int^t (\psi_0(y,-\tau),\,\Omega_0(y,-\tau),\,f_0(-\tau))\,d\tau, \tag{A8}$$

as is readily seen. For convenience, we select the constant C such that

$$\int_d^0 \int_0^{2\pi} \psi_0^* \Omega_0 \, dy \, dt - \int_0^{2\pi} \left[ik_c^{-1}\left(\psi_{0yyy}^* + \psi_{0yt}^* - 3k_c^2 \psi_{0y}^*\right) f_0 + \psi_0^* \psi_{0y}\right]_{y=0} dt = 1. \tag{A9}$$

As a consequence of (2.10)–(2.11) and (A8), we have

$$(\psi_0^*,\,\Omega_0^*)(y,t+\pi) \equiv -(\psi_0^*,\,\Omega_0^*)(y,t), \quad f_0^*(t+\pi) \equiv -f_0^*(t), \tag{A10}$$

which implies, in particular, that $(\psi_0^*,\,\Omega_0^*)(y,t+2\pi) \equiv (\psi_0^*,\,\Omega_0^*)(y,t)$, $f_0^*(t+2\pi) \equiv f_0^*(t)$, and $\langle \psi_0^* \rangle^t \equiv \langle \Omega_0^* \rangle^t \equiv \langle f_0^* \rangle^t \equiv 0$.

The $O(L^{-2})$ coefficients $(\psi_{12},\,\Omega_{12},\,f_{12})$ and $(\psi_{11},\,\Omega_{11},\,f_{11})$ are given by

$$\psi_{12yy} - 4k_c^2 \psi_{12} = \Omega_{12}, \quad \Omega_{12t} = \Omega_{12yy} - 4k_c^2 \Omega_{12} + ik_c(\psi_{0y}\Omega_0 - \psi_0 \Omega_{0y}) \tag{A11}$$

in $-d < y < 0$, with boundary conditions

$$2ik_c\left(\mathscr{G} + 4\mathscr{S}k_c^2\right) f_{12} - \psi_{12yt} - 8ia_c k_c f_{12}\cos 2t - 12k_c^2 \psi_{12y} + \psi_{12yyy}$$
$$= -ik_c\left(\psi_{0y}^2 + k_c^2 \psi_0^2\right) - \left(\psi_{0yyyy} + 3k_c^4 \psi_0\right) f_0, \quad f_{12t} - 2ik_c \psi_{12}$$
$$= 2ik_c \psi_{0y} f_0 \psi_{12yy} + 4k_c^2 \psi_{12} = -\left(\psi_{0yyy} + 5k_c^2 \psi_{0y}\right) f_0 \quad \text{at } y = 0, \tag{A12}$$

$$\psi_{12} = \psi_{12y} = 0 \quad \text{at } y = -d, \tag{A13}$$

$$(\psi_{12},\,\Omega_{12})(y,t+2\pi) \equiv (\psi_{12},\,\Omega_{12})(y,t), \quad f_{12}(t+2\pi) \equiv f_{12}(t),$$

which has a unique solution, and

$$\psi_{11yy} - k_c^2 \psi_{11} = \Omega_{11} - 2k_c \psi_0, \quad \Omega_{11t} = \Omega_{11yy} - k_c^2 \Omega_{11} + 2k_c \Omega_0 \tag{A14}$$

in $-d < y < 0$, with boundary conditions

$$ik_c\left(\mathscr{G} + \mathscr{S}k_c^2\right) f_{11} - \psi_{11yt} - 4ik_c a_c f_{11}\cos 2t - 3k_c^2 \psi_{11y} + \psi_{11yyy}$$
$$= i\left(\mathscr{G} + 3k_c^2 \mathscr{S}\right) f_0 - 4ia_c f_0 \cos 2t - 6k_c \psi_{0y},$$
$$f_{11t} - ik_c \psi_{11} = -i\psi_0, \quad \psi_{11yy} + k_c^2 \psi_{11} = 2k_c \psi_0 \quad \text{at } y = 0, \tag{A15}$$

$$\psi_{11} = \psi_{11y} = 0 \quad \text{at } y = -d, \tag{A16}$$

$$(\psi_{11},\,\Omega_{11})(y,t+2\pi) \equiv (\psi_{11},\,\Omega_{11})(y,t), \quad f_{11}(t+2\pi) \equiv f_{11}(t), \tag{A17}$$

which is singular because its homogeneous counterpart is (2.7)–(2.9). However, this problem is solvable because it exhibits the following particular solution

$$(\psi_{11},\,\Omega_{11},\,f_{11}) = -\left(\psi_{0k_c},\,\Omega_{0k_c},\,f_{0k_c}\right) \equiv -\left(\frac{\partial \psi_0}{\partial k_c},\,\frac{\partial \Omega_0}{\partial k_c},\,\frac{\partial f_0}{\partial k_c}\right), \tag{A18}$$

which is consistent with the fact that k_c corresponds to the minimum of the marginal instability curve, a $vs.$ k (figure 2a). The $O(L^{-3})$ coefficients in (A 3) are given by

$$\psi_{jyy} - k_c^2 \psi_j = \Omega_j - H_{1j}, \quad \Omega_{jt} = \Omega_{jyy} - k_c^2 \Omega_j - \alpha_j \Omega_0 + H_{2j} \qquad (A\,19a,b)$$

in $-d < y < 0$, with boundary conditions

$$ik_c(\mathscr{G} + \mathscr{S}k_c^2)f_j - \psi_{jyt} - 4ia_c k_c f_j \cos 2t - 3k_c^2 \psi_{jy} + \psi_{jyyy} = \alpha_j \psi_{0y} + h_{3j}(t),$$

$$f_{jt} - ik_c \psi_j = -\alpha_j f_0 + h_{1j}, \quad \psi_{jyy} + k_c^2 \psi_j = h_{2j} \quad \text{at} \quad y = 0, \quad (A\,20)$$

$$\psi_j = \psi_{jy} = 0 \quad \text{at} \; y = -d, \qquad (A\,21)$$

$$(\psi_j, \Omega_j)(y, t+2\pi) \equiv (\psi_j, \Omega_j)(y, t), \quad f_j(t+2\pi) \equiv f_j(t), \qquad (A\,22)$$

for $j = 1, \ldots, 4$, where the functions H_{1j}, H_{2j}, h_{1j}, h_{2j} and h_{3j} are given by

$$H_{11} = -2k_c \psi_{11} + \psi_0, \quad H_{21} = -2k_c \Omega_{11} + \Omega_0, \, h_{11} = i\psi_{11}, \quad h_{21} = -2k_c \psi_{11} + \psi_0,$$

$$h_{31} = i(4a_c \cos 2t - \mathscr{G} - 3\mathscr{S}k_c^2)f_{11} + 3i\mathscr{S}k_c f_0 + 6k_c \psi_{11y} - 3\psi_{0y},$$

$$H_{12} = H_{22} = 0, \quad h_{12} = h_{22} = 0, \quad h_{32} = 4ik_c f_0 \cos 2t,$$

$$H_{13} = 0, \quad H_{23} = ik_c(\psi_{12y}\Omega_0 + 2\psi_{12}\Omega_{0y} - 2\psi_{0y}\Omega_{12} - \psi_0 \Omega_{12y}),$$

$$h_{13} = ik_c(\psi_{12y}f_0 - \psi_{0y}f_{12} - k_c^2 \psi_0 f_0^2/2),$$

$$h_{23} = -(\psi_{12yyy} - 4k_c^2 \psi_{12y})f_0 + (\psi_{0yyy} - 7k_c^2 \psi_{0y})f_{12} - (\psi_{0yyyy} - 9k_c^4 \psi_0)f_0^2/2,$$

$$h_{33} = ik_c[\psi_0(\Omega_{12} + 6k_c^2 \psi_{12}) + \psi_{0y}\psi_{12y}] + (3k_c^2 \psi_{0t} + \psi_{0yyyy} + 3k_c^4 \psi_0)f_{12}$$

$$\quad - (2k_c^2 \psi_{12t} - \psi_{12tyy} + \psi_{12yyyy} - 8k_c^2 \psi_{12yy} + 16k_c^4 \psi_{12})f_0 + 3i\mathscr{S}k_c^5 f_0^3/2$$

$$\quad + ik_c(\psi_{0yyy} + 5k_c^2 \psi_{0y})\psi_0 f_0 + [(\psi_{0t} - \psi_{0yy} + k_c^2 \psi_0)_{yyy}/2 + k_c^2 \psi_{0yt} - 5k_c^4 \psi_{0y}]f_0^2,$$

$$H_{14} = H_{24} = 0, \quad h_{14} = ik_c \psi_{0y}, \quad h_{24} = -(\psi_{0yyyy} + k_c^2 \psi_{0y}),$$

$$h_{34} = -(k_c^2 \psi_{0t} + \psi_{0yyy} + 3k_c^4 \psi_0).$$

Here, we have taken into account (2.13). The problem (A 19a, b)–(A 22) is again singular for $j = 1, \ldots, 4$ and thus has solution(s) only if an appropriate solvability condition holds. This consists of requiring that the right-hand sides of (A 19) (A 20) be orthogonal, with an appropriate inner product, to a non-trivial solution of the adjoint homogeneous problem (A 4) (A 6). The coefficients $\alpha_1, \ldots,$ and α_4 are given by

$$\alpha_j = \int_0^{2\pi} \int_{-d}^0 [(\bar{\psi}_{0t}^* + \bar{\Omega}_0^*)H_{1j} + \bar{\psi}_0^* H_{2j}]\,dy\,dt + \int_0^{2\pi} [\bar{\psi}_0^* H_{1jy} - \bar{\psi}_{0y}^* H_{1j}]_{y=0}\,dt$$

$$+ \int_0^{2\pi} \left[-ik_c^{-1}(\bar{\psi}_{0yyy}^* + \bar{\psi}_{0yt}^* - 3k_c^2 \bar{\psi}_{0y}^*)h_{1j} - \bar{\psi}_{0y}^* h_{2j} + \bar{\psi}_0^* h_{3j} \right]_{y=0}\,dt, \quad (A\,23)$$

as obtained by multiplying (A 19b) by $\bar{\psi}_0^*$, multiplying the complex conjugate of (A 4b) by ψ_j, subtracting the resulting equations, integrating in $-d < y < 0$, $0 < t < 2\pi$, integrating by parts repeatedly, substituting the remaining equations and boundary conditions in (A 19)–(A 22) and (A 4)–(A 6), and using (A 9). Applying (A 23) to (A 19)–(A 22) we obtain the coefficients $\alpha_1, \ldots, \alpha_4$, which are as plotted in figure 3. For the sake of brevity, we give here only the explicit expression for α_4, which is

$$\alpha_4 = \int_0^{2\pi} \left[(\bar{\psi}_{0yyy}^* + \bar{\psi}_{0yt}^* - 2k_c^2 \bar{\psi}_{0y}^*)\psi_{0y} + \bar{\psi}_{0y}^* \psi_{0yyy} + k_c^2 \bar{\psi}_0^* \psi_{0t} \right]_{y=0}\,dt$$

$$= -\int_0^{2\pi} [\bar{\psi}_{0yy}^* \psi_{0yy}]_{y=-d}\,dt, \quad (A\,24)$$

where the second equality follows after some algebra using (2.7)–(2.9) and (A 4)–(A 6). Thus, since $\psi_{0yy}(-d) \to 0$ exponentially as $d \to \infty$, (A 24) shows that $\alpha_4 \to 0$ exponentially as $d \to \infty$. Note that $\mathscr{G}$ and $\mathscr{S}$ are assumed to be bounded here; see §A.3 below.

A.2. *Slowly varying terms: second amplitude equation* (3.3)

The mean flow equation is now derived from the following equations, which are obtained by substituting (A 2) and (A 3) into (2.1)–(2.4), taking the spatial mean value in the short spatial variable x, and retaining only leading-order terms,

$$\psi_{yy}^m = \Omega^m, \quad \Omega_{yy}^m = H(y)(|A|^2)_\xi \quad \text{in} \quad -d < y < 0, \tag{A 25}$$

$$f_T^m - \psi_\xi^m = -\alpha_5(|A|^2)_{\xi\xi}, \quad \psi_{yy}^m = \alpha_6(|A|^2)_\xi, \quad \psi_{yyy}^m + \mathscr{G} f_\xi^m = -\alpha_7(|A|^2)_\xi \quad \text{at } y = 0, \tag{A 26a–c}$$

$$\int_0^1 \Omega_y^m \, \mathrm{d}\xi = \psi^m = \psi_y^m = 0 \quad \text{at } y = -d, \quad \int_0^1 f^m \, \mathrm{d}\xi = 0, \tag{A 27}$$

$$(\psi^m, \Omega^m)(\xi + 1, y, T) \equiv (\psi^m, \Omega^m)(\xi, y, T), \quad f^m(\xi + 1, T) \equiv f^m(\xi, T), \tag{A 28}$$

where

$$H(y) = \frac{1}{2\pi} \int_0^{2\pi} \left[\psi_{0y}\Omega_0 - \psi_0\Omega_{0y} + k_c(\psi_{11}\Omega_0 - \psi_0\Omega_{11})_y \right] \mathrm{d}t, \tag{A 29}$$

$$\alpha_5 = \frac{\mathrm{i}}{2\pi} \int_0^{2\pi} \left[\psi_{0y}f_{11} - \psi_{11y}f_0 \right]_{y\,0} \mathrm{d}t, \tag{A 30}$$

$$\alpha_6 = \frac{\mathrm{i}}{2\pi} \int_0^{2\pi} \left[\left(2k_c\psi_{0y} + 3k_c^2\psi_{11y} - \psi_{11yyy} \right) f_0 + \left(\psi_{0yyy} - 3k_c^2\psi_{0y} \right) f_{11} \right]_{y=0} \mathrm{d}t, \tag{A 31}$$

$$\alpha_7 = \frac{1}{2\pi} \int_0^{2\pi} \left[|\psi_{0y}|^2 - k_c^2|\psi_0|^2 + \mathrm{i}\left(2k_c^2\psi_{11t} + \psi_{11yyyy} - 4k_c\psi_{0t} + 3k_c^4\psi_{11} \right) f_0 \right.$$
$$\left. - \mathrm{i}\left(2k_c^2\psi_{0t} + \psi_{0yyyy} + 3k_c^4\psi_0 \right) f_{11} \right]_{y=0} \mathrm{d}t, \tag{A 32}$$

as obtained (after some algebra) using (2.8), (2.13), (A 15) and (A 18). Note that H, α_7, α_5 and α_6 are all real. Integration of (A 25), (A 26) and (A 27) yields

$$\psi^m = \left[\frac{K_1(y + d)^2}{2} - \frac{K_2(y + d)^3}{6} + \frac{1}{6} \int_d^y (y - z)^3 H(z) \, \mathrm{d}z \right] (|A|^2)_\xi$$
$$+ \mathscr{G} \frac{(2d - y)(y + d)^2}{6} f_\xi^m, \tag{A 33}$$

where

$$K_1 = \alpha_6 + \alpha_7 d + \int_d^0 (z - d)H(z) \, \mathrm{d}z, \quad K_2 = \alpha_7 - \int_d^0 H(z) \, \mathrm{d}z. \tag{A 34}$$

And substitution of (A 33) into the boundary condition (A 26a) leads to (A 1a), where β_1 is given by

$$\beta_1 = -\alpha_5 + \frac{\alpha_6 d^2}{2} + \frac{\alpha_7 d^3}{3} + \frac{1}{6} \int_{-d}^0 (3d^2 z - 2d^3 - z^3) H(z) \, \mathrm{d}z, \tag{A 35}$$

and is plotted in figure 3e *vs.* d^2, for the indicated values of $\mathscr{G} d^3$ and $\mathscr{S} d$.

A.3. *Small viscosity*

As viscosity goes to zero, either $\mathscr{G} \gg 1$ or $\mathscr{S} \gg 1$ (see (2.5)), and the wavenumber at threshold is

$$k_c \simeq k_{c0} \sim \left(\mathscr{G} + \mathscr{S}^{1/3} \right)^{-1} \ll 1, \tag{A 36}$$

where k_{c0} is the inviscid approximation of k_c, which obeys the inviscid dispersion relation

$$k_{0c} \left(\mathscr{G} + k_{0c}^2 \mathscr{S} \right) \tanh k_{oc} d = 1. \tag{A 37}$$

For convenience we use the gravity–capillary balance parameter S and the non-dimensional measure of viscous effects ε, defined as

$$S = \frac{k_{0c}^2 \mathscr{S}}{k_{0c}^2 \mathscr{S} + \mathscr{G}} \sim 1, \quad \varepsilon = k_{0c}^2 \ll 1. \tag{A 38}$$

Also, inspection of the expressions derived above (which is fairly tedious and is omitted) shows that

$$\left. \begin{array}{l} \alpha_1^{-1} \sim \alpha_3 \sim \alpha_5^{-1} \sim \varepsilon \alpha_6^{-1} \sim \varepsilon^{3/2} \left(\varepsilon^{1/2} + \mathrm{e}^{-2k_c d} \right), \\ \alpha_2 \sim \alpha_7 \sim y H(y) \sim \varepsilon^{1/2}, \quad \alpha_4 \sim \varepsilon \mathrm{e}^{-2k_c d}. \end{array} \right\} \tag{A 39}$$

These asymptotic estimates have been thoroughly checked numerically (see, e.g. figures 7 and 9). Thus (see (A 35)),

$$\beta_1 \sim \varepsilon^{3/2} \quad \text{as } \varepsilon \to 0. \tag{A 40}$$

Appendix B. Derivation of the NPGL equation (B 6)

In the limit

$$k_c d \to \infty, \tag{B 1}$$

the coefficient α_4 becomes negligible (see (4.1)) and the first amplitude equation (3.3) becomes decoupled from the free-surface elevation. This is true for moderately large d, but not for sufficiently large d, when the horizontal velocity $\psi_y^m \sim d$ is large (see (B 2)) and some terms that, are higher order when $d \sim 1$ become non-negligible in (A 1). In order to see that, we note that, in the limit (B 1),

$$\psi_y^m \simeq \frac{\alpha_6 d}{4} (|A|^2)_\xi, \quad f^m \simeq -\frac{\beta_2}{\mathscr{G}} (|A|^2 - \langle |A|^2 \rangle^\xi), \tag{B 2a, b}$$

where the spatial mean value $\langle \cdot \rangle$ is defined in (B 3) and

$$\beta_2 = \frac{3\beta_1}{d^3} \simeq \alpha_7 - \int_{-\infty}^0 H(z)\,\mathrm{d}z, \tag{B 3}$$

as obtained using (A 33), integrating in (A 1b), and taking into account that α_5, α_6, α_7 and $y H(y)$ remain bounded as $d \to \infty$ if both $\mathscr{G}$ and $\mathscr{S}$ remain finite, while these behave as indicated in (A 39) at small viscosity in deep containers, namely in the combined limit $d \to \infty$, $\varepsilon \to 0$. Substituting (B 2) into (A 3), a new term must be included in the right-hand side of (A 3) that is of the order of d/L^4. The new term is proportional to $\psi_y^m A$ and can be written as

$$\frac{d}{L^4} (|A|^2)_\xi A(\psi_8, \Omega_8, f_8) \mathrm{e}^{\mathrm{i} k_c x}. \tag{B 4}$$

This gives a new term in the right-hand side of (A 1a), which is rewritten as

$$A_T = \alpha_1 A_{\xi\xi} + \alpha_2 \Sigma A + \alpha_3 A|A|^2 + i(\alpha_8/L)\psi_y^m A \tag{B 5}$$

or, invoking (B 2a), as

$$A_T = \alpha_1 A_{\xi\xi} + \alpha_2 \Sigma A + \alpha_3 A|A|^2 + i\frac{\alpha_6\alpha_8}{4}\frac{d}{L}(|A|^2)_\xi A. \tag{B 6}$$

Here, (ψ_8, Ω_8, f_8) and α_8 are given by (A 19) (A 22), with $(j = 8, d = \infty)$, and

$$H_{18} = 0, \quad H_{28} = k_c\Omega_0, \quad h_{18} = k_c f_0, \quad h_{28} = 0, \quad h_{38} = -k_c\psi_{0y}. \tag{B 7}$$

We need only apply a solvability condition (the counterpart of (A 23), with $j = 8$ and $d = \infty$), to this latter problem, to obtain

$$\alpha_8 = k_c \int_0^{2\pi} \left[\int_{-\infty}^0 \bar{\psi}_0^* \Omega_0 \, dy - \left[ik_c^{-1} \left(\bar{\psi}_{0yyy}^* + \bar{\psi}_{0yt}^* - 3k_c^2\bar{\psi}_{0y}^* \right) f_0 + \bar{\psi}_0^* \psi_{0y} \right]_{y=0} \right] dt = k_c,$$

where the last equality comes from invariance under Galilean transformations: $x \rightarrow x - ct$, $\xi \rightarrow \xi - T/L$, $\psi_y \rightarrow \psi_y - c$ (namely, replacing these transformations into (A 3) and (B 5), we obtain a new term on the right-hand side of (B 5), $icL^{-2}(\alpha_8 - k_c)A$, which must vanish). The coefficient α_8 is plotted in figure 7. Note that according to the assumptions above, (2.6), the new non-potential term is small compared to cubic nonlinearity in principle, except when $|\alpha_6\alpha_8|$ is large compared to $|\alpha_3|$, which occurs in particular as viscosity goes to zero, as seen invoking (A 39) and

$$\alpha_8 \sim \varepsilon^{1/2} \quad \text{as } \varepsilon \rightarrow 0. \tag{B 8}$$

Appendix C. Linear stability of the spatially uniform SWs of the amplitude equations

The simplest steady states of the amplitude equations (3.7) (3.8), (3.12) and (4.4), and their linear stability properties can be obtained in closed form.

C.1. *CAMF equations* (3.7) (3.8)

The uniform steady states of (3.7)–(3.8) are given by

$$B = B_n \equiv \sqrt{\mu - \delta_n^2}e^{i\delta_n\xi}, \quad f^m = 0 \quad \text{if } \mu > \delta_n^2 \text{ with } \delta_n = \delta + 2\pi n., \tag{C 1}$$

for $n = 0, \pm 1, \pm 2, \ldots$, and are in branches that bifurcate from the trivial solution $B = f^m = 0$ at $\mu = \delta_n^2$. The linear stability of these is analysed replacing $B - B_n = B_n[Xe^{\lambda\tau - ik_m\xi} + \bar{Y}e^{\lambda\tau - ik_m\xi}]$ and $f^m = |B_n|^2 Ze^{\lambda\tau + ik_m\xi} + \text{c.c.}$, with $k_m = 2\pi m$ for $m = 0, \pm 1, \pm 2, \ldots$, and linearizing, to obtain a linear system of equations that has non-trivial solutions provided that

$$\lambda^3 + \left[(\gamma_1 + 2)k_m^2 + 2|B_n|^2\right]\lambda^2 + \left[(2\gamma_1 + 1)k_m^2 + 2(\gamma_1 + \gamma_2 + 1)|B_n|^2 - 4\delta_n^2\right]k_m^2\lambda$$
$$+ \left[2(\gamma_1 + \gamma_2)|B_n|^2 + \gamma_1\left(k_m^2 - 4\delta_n^2\right)\right]k_m^4 = 0. \tag{C 2}$$

This dispersion relation readily shows that:

(a) If $\gamma_1 + \gamma_2 > 0$ (figure 5a), then the solutions in the first branch $(n = 0)$ are all stable, while those in the remaining branches $(n \neq 0)$ are stable only if $|B_n|^2 > 2\gamma_1(\delta_n^2 - \pi^2)/(\gamma_1 + \gamma_2)$, the instability being stationary $(\lambda = 0)$ provided that $\gamma_1(\gamma_1 + \gamma_2)(\delta_n^2 + \pi^2) \geqslant \gamma_1\pi^2 + \gamma_2\delta_n^2$, and oscillatory $(\lambda = \text{purely imaginary})$ otherwise.

(*b*) If $\gamma_1 + \gamma_2 < 0$ (figure 5*b*), then the solutions in the first branch ($n = 0$) are stable provided that $|B_0|^2 < -2\gamma_1(\pi^2 - \delta^2)/(\gamma_1 + \gamma_2)$, and unstable otherwise; the solutions in the remaining branches are all unstable.

C.2. *NLGL equation* (3.12)

The uniform steady states are again given by (C 1), namely

$$B = B_n \equiv \sqrt{\mu - \delta_n^2}\,e^{i\delta_n\xi} \quad \text{for } \mu > \delta_n^2 \text{ with } \delta_n = \delta + 2\pi n. \tag{C 3}$$

The linear stability of these is analysed as above, substituting

$$B - B_n = B_n[Xe^{\lambda\tau - ik_m\xi} + \bar{Y}e^{\bar{\lambda}\tau - ik_m\xi}] \tag{C 4}$$

into (3.12) and linearizing. It follows that the dispersion relation is given by

$$\lambda^2 + 2R_n^2\lambda = 0 \quad \text{if } m = 0, \tag{C 5}$$

$$\left(\lambda + k_m^2\right)^2 + 2(1 + \Gamma)R_n^2\left(\lambda + k_m^2\right) = 4k_m^2\delta_n^2 \quad \text{if } m \leqslant 0, \tag{C 6}$$

and implies that the first branch ($n = 0$) is exponentially stable, while the remaining branches ($n \neq 0$) are exponentially stable if $(1 + \Gamma)R_n^2 > 2(k_n^2 - \pi^2)$, and unstable otherwise. This gives the plot in figure 5(*a*) if $1 + \Gamma > 0$.

C.3. *NPGL equation* (4.4)

The uniform steady states of (4.4) are given once more by (C 3) and their linear stability is analysed replacing (C 4) into (4.4) and linearizing. The dispersion relation is

$$\left(\lambda + k_m^2\right)^2 + 2\left(\lambda + k_m^2\right)R_n^2 - 4\gamma D\delta_n k_m^2 R_n^2 - 4\delta_n^2 k_m^2 = 0, \tag{C 7}$$

and shows that (figure 8):

(i) The whole first branch ($n = 0$) is exponentially stable if $2\gamma D\delta \leqslant 1$. If instead $2\gamma D\delta > 1$, then this branch is exponentially stable for $R_0^2 < 4(\pi^2 - \delta^2)/(2\gamma D\delta - 1)$ and unstable otherwise, the instability being stationary ($\lambda = 0$).

(ii) The remaining branches with $n \neq 0$ are stable if $2\gamma D\delta_n < 1$ and $R_n^2 > 4(\delta_n^2 - \pi^2)/(1 - 2\gamma D\delta_n)$ and are unstable otherwise, the instability being stationary ($\lambda = 0$).

(iii) Note in particular that if $0 < \delta < \pi$ and γD is sufficiently large, then the first branch is stable only in a vicinity quite close to threshold, $\delta^2 < \mu < \mu_0' = \delta^2 + 4(\pi^2 - \delta^2)/(2\gamma D\delta - 1) < (2\pi - \delta)^2 = \mu_{-1}$. In this case, no steady state with a constant amplitude is stable in the interval $\mu_0' < \mu < \mu_{-1}$.

REFERENCES

BATCHELOR, G. K. 1967 *An Introduction to Fluid Dynamics*. Cambridge University Press.

BECHHOEFER, J., EGO, V., MANNEVILLE, S. & JOHNSON, B. 1995 An experimental study of the onset of parametrically pumped surface waves in viscous fluids. *J. Fluid Mech.* **288**, 325–350.

BENJAMIN, T. B. & GRAHAM-EAGLE, J. 1985 Long gravity capillary waves with edge constraints. *IMA J. Appl. Maths* **35**, 91–114.

BENJAMIN, T. B. & SCOTT, S. 1979 Gravity capillary waves with edge constraints. *J. Fluid Mech.* **92**, 241–267.

BEYER, J. & FRIEDRICH, R. 1995 Faraday instability: linear analysis for viscous fluids. *Phys. Rev. E* **51**, 1162–1168.

CERDA, E. & TIRAPEGUI, E. 1998 Faraday's instability in viscous fluid. *J. Fluid Mech.* **368**, 195–228.

CHANDRASEKHAR, S. 1961 *Hydrodynamic and Hydromagnetic Stability*. Clarendon.

CHEN, P. & VIÑALS, J. 1999 Amplitude equation and pattern selection in Faraday waves. *Phys. Rev. E* **60**, 559–570.

COULLET, P. & IOOSS, G. 1990 Instabilities of one-dimensional cellular patterns. *Phys. Rev. Lett.* **64**, 866–869.

CROSS, M. C. & HOHENBERG, P. C. 1993 Pattern formation outside of equilibrium. *Rev. Mod. Phys.* **65**, 851–1112.

DAVEY, A. & STEWARTSON, K. 1974 On three-dimensional packets of surface waves. *Proc. R. Soc. Lond.* A **338**, 101 110.

DAVEY, A., HOCKING, L. M. & STEWARTSON, K. 1974 On nonlinear evolution of three-dimensional disturbances in plane Poiseuille flow. *J. Fluid Mech.* **63**, 529 536.

DOUADY, S., FAUVE, S. & THUAL, O. 1989 Oscillatory phase modulation of parametrically forced surface waves. *Europhys. Lett.* **10**, 309–315.

ELMER, F. J. 1988 Nonlinear and nonlocal dynamics of spatially extended systems: stationary states, bifurcations and stability. *Physica* D **30**, 321–342.

FARADAY, M. 1831 On the forms and states assumed by fluids in contact with vibrating elastic surfaces. *Phil. Trans. R. Soc. Lond.* **121**, 319 340.

FAUVE, S. 1995 Parametric instabilities. In *Dynamics of Nonlinear and Disordered Systems* (ed. G. Martinez-Mekler & T. H. Seligman) pp. 67 115. World Scientific.

GOLOVIN, A. A., NEPOMNYASHCHY, A. A. & PISMEN, L. M. 1994 Interaction between short-scale Marangoni convection and long-scale deformational instability. *Phys. Fluids* **6**, 34–48.

HANSEN, P. L. & ALSTROM, P. 1997 Perturbation theory of parametrically driven capillary waves at low viscosity. *J. Fluid Mech.* **351**, 301–344.

HIGUERA, M., VEGA, J. M. & KNOBLOCH, E. 2002 Coupled amplitude-mean flow equations for nearly-inviscid Faraday waves in moderate aspect ratio containers. *J. Nonlinear Sci.* **12**, 505–551.

HOFFMANN, F. M. & WOLF, G. H. 1974 Excitation of parametric instabilities in statically stable and unstable fluid interfaces. *J. Appl. Phys.* **45**, 3859 3863.

KNOBLOCH, E. 1995 Remarks on the use and misuse of the Ginzburg–Landau equation. In *Nonlinear Dynamics and Pattern Formation in the Natural Environment* (ed. A. Doelman & A. van Harten), pp. 130 146. Longman.

KUDROLLI, A. & GOLLUB, J. P. 1997 Patterns and spatio-temporal chaos in parametrically forced surface waves: a systematic survey at large aspect ratio. *Physica* D **97**, 133–154.

KUMAR, K. & TUCKERMAN, L. S. 1994 Parametric instability of the interface between two fluids. *J. Fluid Mech.* **279**, 49 68.

LAPUERTA, V., MANCEBO, F. J. & VEGA, J. M. 2001 Control of Rayleigh–Taylor instability by vertical vibration in large aspect ratio containers. *Phys. Rev.* E **64**, 016318-1-17.

LAPUERTA, V., MARTEL, C. & VEGA, J. M. 2002 Interaction of nearly-inviscid Faraday waves and mean flows in 2-D containers of quite large aspect ratio. *Physica* D **173**, 178–203.

LIOUBASHEVSKI, O., FINEBERG, J. & TUCKERMAN, L. S. 1997 Scaling of the transition to parametrically driven surface waves in highly dissipative systems. *Phys. Rev.* E **55**, R3832–R3835.

MANCEBO, F. J. & VEGA, J. M. 2002 Faraday instability threshold in large aspect ratio containers. *J. Fluid Mech.* **467**, 307 330.

MANCEBO, F. J. & VEGA, J. M. 2004 Standing wave description of nearly-conservative, parametrically driven waves in extended systems. *Physica* D **197**, 346–363.

MARTEL, C. & VEGA, J. M. 1996 Finite size effects near the onset of the oscillatory instability. *Nonlinearity* **9**, 1129–1171.

MARTÍN, E., MARTEL, C. & VEGA, J. M. 2002 Drift instability of standing Faraday waves in an annular container. *J. Fluid Mech.* **467**, 57–79.

MATTHEWS, P. C. & COX, S. M. 2000 Pattern formation with a conservation law. *Nonlinearity* **13**, 1293 1320.

MILES, J. & HENDERSON, D. 1990 Parametrically forced surface waves. *Annu. Rev. Fluid Mech.* **22**, 143–165.

MÜLLER, H. W., WITTMER, H., WAGNER, C., ALBERS, J. & KNORR, K. 1997 Analytic stability theory for Faraday waves and the observation of the harmonic surface response. *Phys. Rev. Lett.* **78**, 2357–2360.

NORBURY, J., WEI, J. & WINTER, M. 2002 Existence and stability of singular patterns in a Ginzburg–Landau equation coupled with a mean field. *Nonlinearity* **15**, 2077–2096.

RAYLEIGH, LORD 1883 On the crispations of fluid resting upon a vibrating support. *Phil. Mag.* **16**, 50–58.

VEGA, J. M. 2005 Instability of the steady states of some Ginzburg–Landau-like equations with real coefficients. Nonlinearity **18**, 1425–1441.

VEGA, J. M. & KNOBLOCH, E. 2003 Dynamics of counterpropagating waves in parametrically forced, large aspect ratio, nearly conservative systems with nonzero detuning. *Fluid Dyn. Res.* **33**, 113–140.

VEGA, J. M., KNOBLOCH, E. & MARTEL, C. 2001 Nearly inviscid Faraday waves in annular containers of moderately large aspect ratio. *Physica* D **154**, 313–336.

VEGA, J. M., RÜDIGER, S. & VIÑALS, J. 2003 A phenomenological model of weakly damped Faraday curves and the associated mean flow. *Phys. Rev.* E **70**, 046306.

WESTRA, M.-T., BINKS, D. J. & VAN DE WATER, W. 2003 Patterns of Faraday waves. *J. Fluid Mech.* **496**, 1–3.

ZHANG, W. & VIÑALS, J. 1997 Pattern formation in weakly damped parametric surface waves. *J. Fluid Mech.* **336**, 301–330.

ZIPPELIUS, A. & SIGGIA, E. 1982 Disappearance of stable convection between free-slip boundaries. *Phys. Rev.* A **26**, 1788–1790.